Modelling and finite element analysis of cavitation and isochoric failure of hyperelastic adhesives

A. Nelson & A. Matzenmiller
Department of Mechanical Engineering, Institute of Mechanics, University of Kassel, Kassel, Germany

ABSTRACT: Finite element analysis is an established tool for the industrial design of adhesively bonded structures. Physical reliable predictions of the load capacity of bonded structures are only possible if suitable constitutive models including the failure are used for the adhesive. Test data of the adhesive to be modelled show rubber-like nonlinear elastic behaviour. Failure is experimentally found to be caused by two different mechanisms, depending on the geometrical shape of the adhesive layer and the load conditions. In order to describe the measured behaviour, a hyperelastic material model is chosen and extended with a damage model to take volumetric and isochoric failure into account. Based on test data, an identification procedure for the elastic and the failure parameters is described. To validate the model, the loading of a component-like specimen is simulated and the results are compared with the corresponding test data.

1 INTRODUCTION

The BETAFORCE 2850 of the DOW Chemical Company is a rubber-like adhesive which is used in a wide range of industrial areas, such as bonding of windshields and joining of structural components in automotive applications. This adhesive is suitable to compensate considerably different deformations of adherends due to its ability to withstand large elastic deformations. Depending on the application, failure can be caused by isochoric as well as volumetric deformations. That has to be taken into consideration properly with a constitutive model.

Developing constitutive models for the industrial application is a combined experimental, analytical and numerical task. The experimental part is regarded as the basis. In what follows, firstly, the experimental program is explained and the finite element representation of used specimens is described. Subsequently, the constitutive equations for the adhesive are shown and motivated. Then, the model parameters are identified. Finally, verification and validation analyses are carried out with the finite element code LS-DYNA using an explicit time integration scheme.

2 TESTS AND FE-MODELLING

The quasistatic behaviour of four specimens is investigate with displacement-controlled tests which finite element models are depicted in figure 1. All adherends consist of steel and are modelled with linear elastic material. The displacement boundary conditions are imposed through either bolts or clamps, which both are modelled as rigid bodies. One of the rigid bodies is fixed and the other one is used to prescribe the boundary condition in z-direction. The discretization of the adhesive layers is as equal as possible for all specimens, i. e. , in-layer element edges are 1 mm and over-thickness element size is $0,5$ mm. The equal discretisation is a deliberate choice to account for (damage) localisation phenomena.

2.1 *Tests with isochoric deformations*

The uniaxial tensile specimen and the thick adherend shear specimen are used for the idenfication of the elasticity constants and the failure parameters of the isochoric part of the material model. The tensile specimen is standardised in DIN 53504 (shape S) and is designed to create a homogeneous tensile stress state in the gauge. Its geometry enables a transverse contraction in the gauge and thereby reduces significantly the hydrostatic pressure so that the influence of the bulk modulus on the stress state is negligible. The deformation is described with the deformation gradient using the transverse nominal strain ε_t and the lateral nominal strain ε

$$\mathbf{F}^{\text{tensile}} = (1-\varepsilon_t)\mathbf{e}_x \otimes \mathbf{e}_x + (1-\varepsilon_t)\mathbf{e}_y \otimes \mathbf{e}_y + \\ +(1+\varepsilon)\mathbf{e}_z \otimes \mathbf{e}_z, \qquad (1)$$

where $\mathbf{e}_i \otimes \mathbf{e}_j$, $i,j = x,y,z$ are the unity dyads with respect to the depicted coordinate systems.

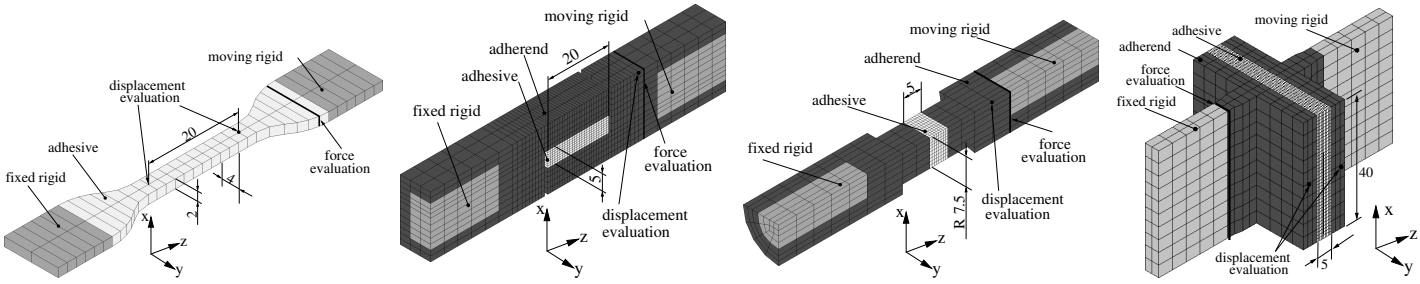

Figure 1: Discretization and dimensioning of (from left to right) the uniaxial tension specimen, the thick adherend shear specimen (half specimen is used), the buttjoint specimen (quater specimen is used) and the T-joint specimen

The thick adherend shear specimen according to DIN EN 14869-2 is tested with two adhesive layer geometries with equal ratios of overlap length to thickness. One test is conducted for an adhesive layer with an area of 20x20 mm and a thickness of 5 mm and the second one with an area of 20x8 mm and a thickness of 2 mm. Symmetry is exploited to increase the computational efficiency. Assuming a homogeneous simple shear deformation and using κ as the tangent of the shear angle, the deformation gradient

$$\mathbf{F}^{\text{shear}} = \mathbf{e}_x \otimes \mathbf{e}_x + \mathbf{e}_y \otimes \mathbf{e}_y + \mathbf{e}_z \otimes \mathbf{e}_z + \kappa\, \mathbf{e}_y \otimes \mathbf{e}_z \quad (2)$$

describes the kinematics analytically.

2.2 *Tests with volumetric deformations*

The buttjoint specimen according to DIN EN 26922 is used to identify the bulk modulus and the failure parameters of the volumetric part of the damage model. The "poker-chip" shaped adhesive layer is tested with a diameter of 15 mm and thicknesses of 1 mm, 2 mm, and 5 mm. Computational efficiency is increased by exploiting symmetry and simulating one quarter of the full geometry. The deformation of the adhesive is inhomogeneous due to the transverse contraction and the geometrical constraint caused by the adherends. Thus, the stress state is a combination of an isochoric and an volumetric part, which contributions depend on the adhesive layer thickness. This is a crucial point which will be exploited for the inverse identification of the bulk modulus in section 4.1.

2.3 *Test of a component-like specimen*

The T-joint specimen is considered as a component-like specimen and therefore is used to validate the constitutive model. The cuboidal adhesive layer has an area of 40x40 mm and a thickness of 5 mm.

3 EXPERIMENTALLY BASED CONSTITUTIVE APPROACH

The adhesive is known to behave rubber-like so that the theory of hyperelasticity is applicable. However, there are still uncertainties regarding the amount of compressibility, i. e. the ratio of the bulk modulus to the shear modulus. Therefore, experimental and analytical studies are performed to confirm the assumption of nearly incompressibility. Based on that, a strain energy density for the hyperelastic model is chosen. Next, the failure behaviour of the adhesive is considered experimentally and numerically using test data and elastic FE-analyses. These results of the elastic analyses are exploited to develop a failure criterion.

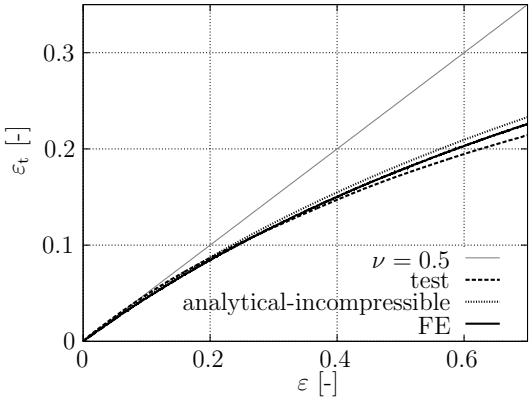

Figure 2: Transversal nominal strain against lateral nominal strain from test, analytical consideration assuming incompresibility and FE-simulation with nearly incompressible behaviour (test data provided by IFAM, Bremen)

3.1 *Consideration of the compressibility*

The compressibility behaviour is studied experimentally by measuring the lateral and the transverse displacements of the uniaxial tensile specimen under loading. Assuming isotropy, figure 2 shows the transverse nominal strain plotted against the lateral nominal strain. With the incompressibility constraint $J = 1$, the kinematics of the uniaxial tensile specimen in equation (1) leads to the analytical expression

$$\varepsilon_t = 1 - \sqrt{\frac{1}{1+\varepsilon}}. \quad (3)$$

The small deviations between the analytical and test results confirm that nearly incompressibility is a reasonable assumption for the considered material.

3.2 *Hyperelastic model*

The model approach is based on the volumetric-isochoric split (Flory 1961) of the deformation gradient

$$\mathbf{F} = \bar{\mathbf{F}} \cdot \hat{\mathbf{F}}, \quad \bar{\mathbf{F}} = J^{-1/3}\mathbf{F}, \quad \hat{\mathbf{F}} = J^{1/3}\mathbf{1}, \tag{4}$$

in which $J = III_F = \det(\mathbf{F})$ is the volume ratio and $\mathbf{1}$ the second order identity tensor. The combination of equation (4) and the definition of the left CAUCHY-GREEN deformation tensor $\mathbf{B} = \mathbf{F} \cdot \mathbf{F}^{\mathrm{T}}$ defines the isochoric left CAUCHY-GREEN deformation tensor

$$\bar{\mathbf{B}} = J^{-2/3}\mathbf{B}, \tag{5}$$

which is used for the definition of the isochoric part of the strain energy density function. Applying the representation theorem for invariants, the strain energy density function for the nearly incompressible adhesive reads as

$$W(I_{\bar{B}}, II_{\bar{B}}, J) = W_{\mathrm{iso}}(I_{\bar{B}}, II_{\bar{B}}) + W_{\mathrm{vol}}(J), \tag{6}$$

where $I_{\bar{B}} = \mathrm{tr}(\bar{\mathbf{B}})$ and $II_{\bar{B}} = \frac{1}{2}\left(\mathrm{tr}(\bar{\mathbf{B}})^2 - \mathrm{tr}(\bar{\mathbf{B}}^2)\right)$ denote the main invariants. The MOONEY-RIVLIN model

$$W_{\mathrm{iso}}(I_{\bar{B}}, II_{\bar{B}}) = \frac{1}{2}c_{10}(I_{\bar{B}} - 3) + \frac{1}{2}c_{01}(II_{\bar{B}} - 3) \tag{7}$$

with the MOONEY-RIVLIN parameters c_{10} and c_{01} is chosen for the isochoric part. From the standpoint of industrial application, this is a reasonable compromise between accuracy and simplicity (and thus efficiency). The chosen ansatz for the volumetric part

$$W_{\mathrm{vol}}(J) = K(J - 1 - \ln J) \tag{8}$$

is adopted from (Miehe 1994) with the bulk modulus K. The effective CAUCHY stresses are calculated by the derivative of the strain energy density function with respect to the left CAUCHY-GREEN deformation tensor

$$\begin{aligned}\hat{\mathbf{T}} =& 2\frac{1}{J}\mathbf{B}\frac{dW(I_{\bar{B}}, II_{\bar{B}}, J)}{d\mathbf{B}} \\ =& \frac{1}{J}\left((c_{10} + c_{01}I_{\bar{B}})\,\bar{\mathbf{B}}^{\mathrm{D}} - c_{01}\left(\bar{\mathbf{B}}^2\right)^{\mathrm{D}}\right) \\ &+ \frac{1}{J}K(J-1)\mathbf{1},\end{aligned} \tag{9}$$

in which $\bar{\mathbf{B}}^{\mathrm{D}}$ is the deviatoric part of the left CAUCHY-GREEN deformation tensor.

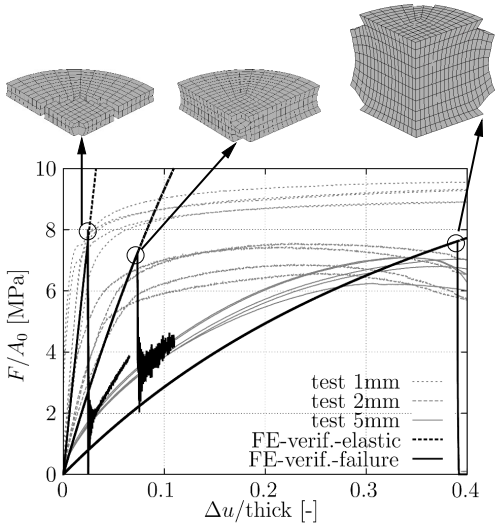

Figure 3: Verification results of the elastic range for the buttjoint specimen

3.3 *Occurence of cavitation*

Rubber-like materials can withstand high pressure under compressional load. Under dilatational load internal rupture known as cavitation occurs. Cavitation is nucleated by so called precursors in the interior of the material and forms enclosed cracks when a critical dilatational load is applied. These cracks tear open at the center, from where they expand. Thus, there is no possibility of visible detection from the outside. However, two measurable phenomena are associated with cavitation. The first is an audible cracking sounds. The second is a significant decrease of the bulk modulus, i. e., a sudden change in the load-extension response.

The experimental results of the buttjoint specimen indicate two failure mechanisms depending on the layer thickness t_{a}. For $t_{\mathrm{a}} = 5$ mm, a crack starts to grow slowly from the outside at a relative displacement of 0.3. In contrast to that, no crack is observed at the outside if $t_{\mathrm{a}} = 2$ mm and $t_{\mathrm{a}} = 1$ mm. The separation of the adherends and thus the fracture of the adhesive appears suddenly. In figure 3, results of the elastic FE-analyses are marked with dashed lines. The calculated curves are in the scatter range of the test data until about 6 MPa for $t_{\mathrm{a}} = 2$ mm and 7 MPa for $t_{\mathrm{a}} = 1$ mm. It is assumed, that the deviations are due to the occurrence of cavitation in the adhesive layers. These failure states are elaborated more concisely concerning the energy state at the corresponding critical locations. To this end, the isochoric, volumetric and total energies for 1 mm, 2 mm, and 5 mm are evaluated and plotted along the radial and axial directions in figure 4. For $t_{\mathrm{a}} = 5$ mm the total energy at the outide, where failure starts, is almost equal to the isochoric energy. In both other cases, $t_{\mathrm{a}} = 2$ mm and $t_{\mathrm{a}} = 1$ mm, the total energy state at the center is dominated by the volumetric energy. Consequently, the volumetric energy is an adequate choice to model cavitation, whereas the isochoric energy is appropriate to model isochoric failure.

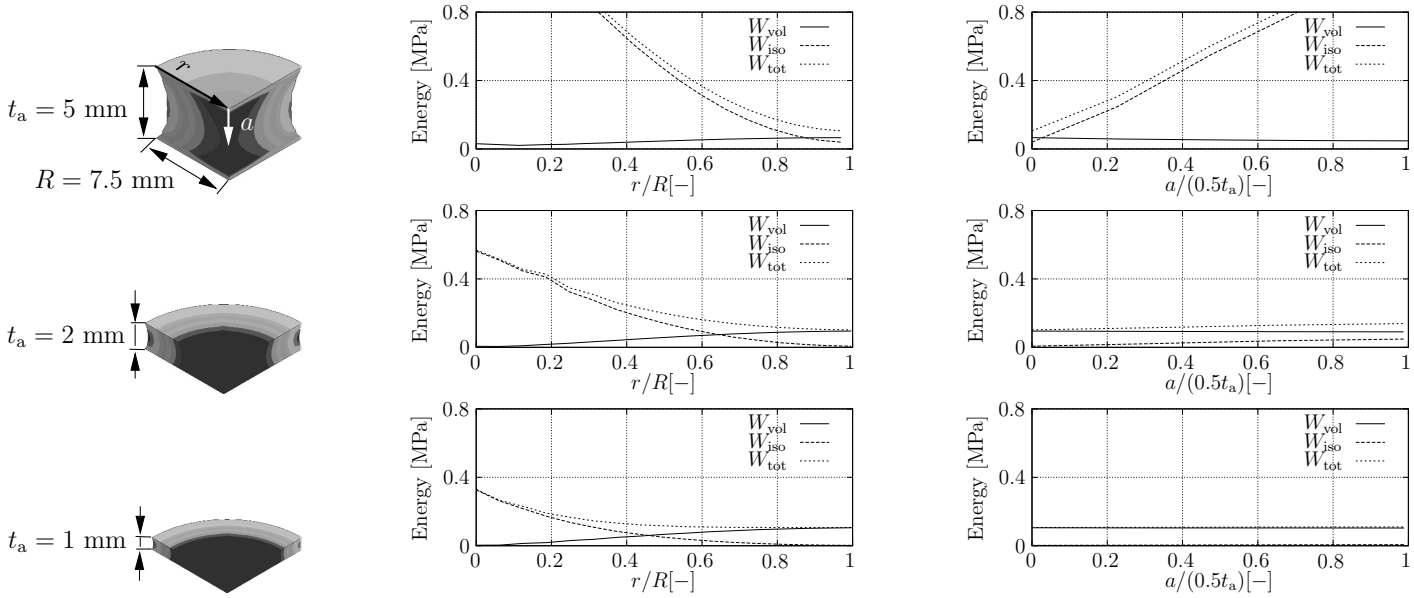

Figure 4: Pressure contour plot (-8 MPa$< p < -0.1$ MPa) for the buttjoint specimen at failure with radial and axial distribution of isochoric, volumetric and total energies. First line $t_a = 5$ mm, second line $t_a = 2$ mm, third line $t_a = 1$ mm (test data provided by LWF, Paderborn)

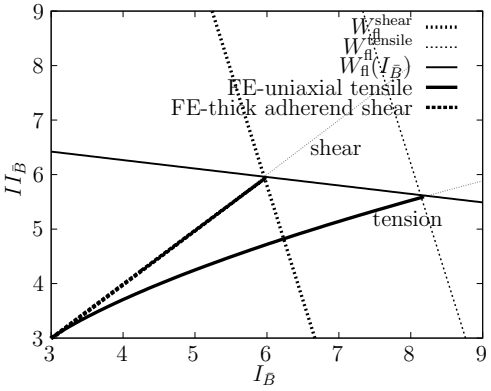

Figure 5: $II_{\bar{B}} - I_{\bar{B}}$-space for isochoric deformations

3.4 *Failure model*

The failure model is based on the continuum damage mechanical concept (Kachanov 1958)

$$\mathbf{T} = (1 - D)\hat{\mathbf{T}}, \tag{10}$$

with the damage variable D acting on the effective stresses according to equation (9). The chosen approach for the damage function is proposed in (Lemaitre 1985)

$$D = \begin{cases} 0, & f \leq W_{\text{fl}} \\ \left\langle \dfrac{f - W_{\text{fl}}}{W_{\text{fc}} - W_{\text{fl}}} \right\rangle, & W_{\text{fl}} < f < W_{\text{fc}} \\ 1, & f \geq W_{\text{fc}} \end{cases} \tag{11}$$

In equation (11) the argument is the equivalent energy

$$f(I_{\bar{B}}, II_{\bar{B}}, J) = W_{\text{iso}}(I_{\bar{B}}, II_{\bar{B}}) + f_{\text{k}} W_{\text{vol}}(J) \tag{12}$$

which is driven by isochoric and volumetric energies. The model parameter f_{k} serves as a multiplier for the contribution of the volumetric energy to f. The mathematical form of the damage function implies the failure criterion

$$f(I_{\bar{B}}, II_{\bar{B}}, J) = W_{\text{fl}} \tag{13}$$

and the fracture criterion

$$f(I_{\bar{B}}, II_{\bar{B}}, J) = W_{\text{fc}}, \tag{14}$$

with W_{fl} and W_{fc} denoting the failure and the fracture energies. They both have to be determined based on test results. In the following, it will be shown that the constant approaches in equations (13) and (14) are unsuitable for the modelling of more than one loading condition. The shortcoming will be elaborated only for the failure criterion. However, the same arguments are applicable for the fracture criterion.

For the simple tension and the simple shear, the relations $II_{\bar{B}}(I_{\bar{B}})$ are derived from the corresponding deformation gradients and plotted as grey dotted curves in figure 5, assuming isochoric deformations. Moreover, FE results of the uniaxial tensile specimen and the thick adherend shear specimen until the onset of failure (at the critical element) are plotted as thick dashed and solid lines. The FE-analyses are assumed to predict the elastic behaviour correctly, which will be addressed in section 4.2. Thus, the corresponding failure energy for tensile $W_{\text{fl}}^{\text{tensile}}$ MPa and for shear $W_{\text{fl}}^{\text{shear}}$ MPa can be extracted from the analyses. Next, the strain energy density from equation (7) and the failure criterion from (13) are inserted in (12) and the resulting expression is solved for $II_{\bar{B}}$ leading to

$$II_{\bar{B}} = \frac{2(W_{\text{fl}} - f_{\text{k}} W_{\text{vol}}(J)) - c_{10}(I_{\bar{B}} - 3)}{c_{01}} + 3. \tag{15}$$

Equation (15) is depicted in the $II_{\bar{B}} - I_{\bar{B}}$-space (see figure 5) under the assumption of isochoric deformations as a thick dotted line for $W_{\text{fl}} = W_{\text{fl}}^{\text{shear}}$ and as a

thin dotted line for $W_{\text{fl}} = W_{\text{fl}}^{\text{tensile}}$. The intersections of the "failure-lines" with the lines corresponding to the tensile load and the shear load show, that either the tensile load or the shear load is described adequately. A reasonable model has to meet both points. Therefore, the failure criterion W_{fl} and the fracture criterion W_{fc} are extended as

$$W_{\text{fl}} = a_1 + a_2 I_{\bar{B}} \tag{16}$$

and

$$W_{\text{fc}} = b_1 + b_2 I_{\bar{B}}. \tag{17}$$

The coefficients a_1, a_2, b_1 and b_2 are used to fit the curves in the $II_{\bar{B}} - I_{\bar{B}}$-space to test data. Practically, a_1 and a_2 in function (16) are computed via

$$\begin{bmatrix} 1 & I_{\text{fl}}^{\text{tensile}} \\ 1 & I_{\text{fl}}^{\text{shear}} \end{bmatrix} \begin{bmatrix} a_1 \\ a_2 \end{bmatrix} = \begin{bmatrix} W_{\text{fl}}^{\text{tensile}} \\ W_{\text{fl}}^{\text{shear}} \end{bmatrix} \tag{18}$$

in which $W_{\text{fl}}^{\text{tensile}}$ and $W_{\text{fl}}^{\text{shear}}$ are the failure energies for tension and shear. $I_{\text{fl}}^{\text{tensile}}$ and $I_{\text{fl}}^{\text{shear}}$ are the corresponding first invariants. An analogue equation counts for the coefficients b_1 and b_2 by interchanging the indices $_{\text{fl}}$ by $_{\text{fc}}$ in equation (18). In summary, the model parameters are $W_{\text{fl}}^{\text{tensile}}$, $W_{\text{fl}}^{\text{shear}}$, f_{k}, $W_{\text{fc}}^{\text{tensile}}$ and $W_{\text{fc}}^{\text{shear}}$, the last two of which serve for the description of post critical behaviour.

Two properties of the failure model shall be emphasised. Firstly, the choice of the approaches in equations (16) and (17) with exactly two coefficients is deliberate, given that the used test data basis consists of two tests. However, the polynomial form is not mandatory and is chosen due to its simplicity. Secondly, the failure function in equation (15) is derivable for other strain energy density functions than the MOONEY-RIVLIN model. However, the function will in general lose its linearity.

4 PARAMETER IDENTIFICATION AND VERIFICATION

The identification of the elastic model parameters and the failure parameters is performed in a consecutive order with test data of the specimens presented in sections 2.1 and 2.2.

4.1 *Identification of elastic parameters*

The three parameters c_{01}, c_{10} and K of the hyperelastic model (9) are identified in two steps using the elastic ranges of test data. The specimens of the uniaxial simple tensile test and the thick adherend shear test are suitable for the identification of the MOONEY-RIVLIN parameters due to their isochoric deformations of the adhesive and consequently independence of the bulk modulus. At first, the shear modulus G is identified using the test data of the shear specimen, see figure 6(right). The Relation $G = c_{01} + c_{10}$ is exploited as a constraint condition for the inverse identification of the MOONEY-RIVLIN parameters c_{01} and c_{10} using the results from the uniaxial tensile test in figure 6(center). The identified parameters are $c_{10} = 4.2$ MPa and $c_{01} = 1$ MPa. The bulk modulus K is identified inversely using the test results of the buttjoint specimen with different thicknesses of the adhesive layer. For a "poker-chip" shaped specimen the contribution of the hydrostatic stresses to the total stress state increases with increasing ratio of diameter to thickness. The critical value of the aspect ratio for a nearly incompressible material ($\nu = 0.49$) for which the stress is essentially hydrostatic is stated to be 15 (e.g. (Dorfmann, Fuller, & Ogden 2002)). The adhesive layers of the buttjoint specimen used in this work are 1 mm, 2 mm, and 5 mm which correspond to ratios of $15, 7.5$ and 3. In figure 3 calculation results are compared with test data for the identified bulk modulus of $K = 1298$ MPa.

4.2 *Identification of failure parameters*

In this work the focus is on the computation of the failure. The post critical behaviour will be addressed in future investigations. The damage model in equation (11) reduces to a failure model by setting $W_{\text{fc}} = 1.01 W_{\text{fl}}$. In this case the three parameters left to identify are the tensile failure energy $W_{\text{fl}}^{\text{tensile}}$, shear failure energy $W_{\text{fl}}^{\text{shear}}$, and the multiplier for the contribution of the volumetric energy f_{k}. The failure energies are identified inversely using test data of the uniaxial tensile test and the thick adherend shear specimen. To this end, FE-analyses of the uniaxial tensile specimen and the thick adherend shear specimen with 5 mm thickness are performed until failure occurs in a critical element and the invariant paths $II_{\bar{B}}(I_{\bar{B}})$ are evaluated as well as the corresponding energies $W_{\text{fl}}^{\text{tensile}} = 12.1$ MPa and $W_{\text{fl}}^{\text{shear}} = 7.7$ MPa. Evaluating equation (18) with these values, the unknown coefficients a_1 and a_2 are computed. The failure criterion is plotted in the $II_{\bar{B}} - I_{\bar{B}}$-space in figure 5 as a thin solid line. In figure 6(center and right) the test data are compared to these simulation results (dashed black lines). Finally, the multiplier $f_{\text{k}} = 17$ is identified using the test data of the buttjoint specimen.

4.3 *Verification*

In figure 6 the final set of parameters is verified by comparing results of verification simulations (solid, black lines) with corresponding test data of the 5 mm buttjoint test, the uniaxial tensile test and the thick adherend test. For increasing values of the multiplier f_{k}, the contribution of the volumetric energy to the equivalent energy f increases and therefore a premature failure can occur for isochoric deformations with very small volumetric contributions. In Figure 3 the multiplier f_{k} is verified quantitatively by the comparison of simulation results (dashed solid lines) with test data

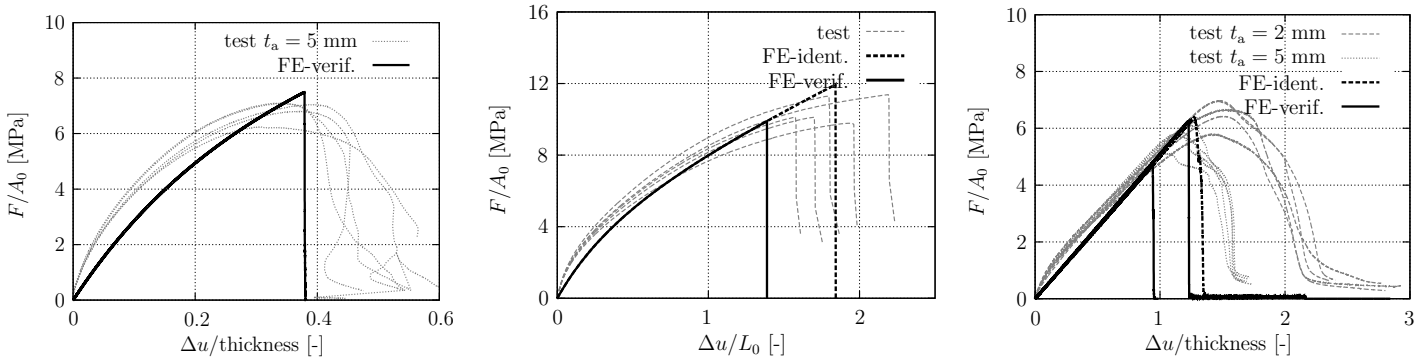

Figure 6: Verification results of buttjoint specimen, uniaxial tensile specimen and thick adherend shear specimen (test data provided by LWF, Paderborn)

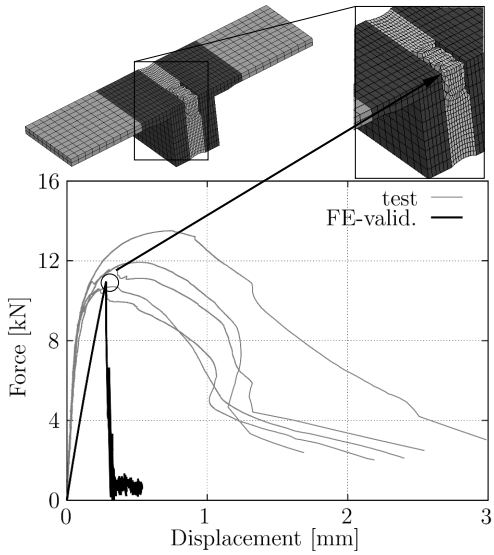

Figure 7: Validation results of the T-joint specimen (test data provided by IFAM, Bremen)

for the buttjoint specimen. Qualitatively, for $t_a = 2$ mm and $t_a = 1$ mm, cavitation is predicted correctly at the center of the adhesive layer. For $t_a = 5$ mm, isochoric failure starts at the outside of the adhesive layer.

5 VALIDATION

The comparison between the numerical results and the test data from the uniaxial tensile specimens in figure 2 can be regarded as a validation for the identified bulk modulus.

The T-joint specimen in figure 1(right) is considered as a validation example for the failure model. In figure 7 the measured data are compared to computed results. In the tests, no crack is detectable at the outside of the specimen, i. e. cavitation starts from the inside and leads to structural failure. Qualitatively, this observation can be confirmed numerically, where the failure starts at the center of the adhesive layer (see FE-model in Figure 7). Quantitatively, the maximum load capacity of about 11 kN is in good agreement with the test data.

6 CONCLUSIONS

For the industrially relevant rubber-like adhesive BETAFORCE 2850 of the DOW Chemical Company the hyperelastic MOONEY-RIVLIN model is extended with a damage model to account for cavitation and isochoric failure. The constitutive equations are implemented into the finite element code LS-DYNA. Using test data, the model parameters are identified and verification analyses are performed. The subsequent validation analysis of a component-like specimen confirms the ability of the model to predict the failure for industrial applications.

ACKNOWLEDGEMENTS

The IGF-project 18716 N/2 of the Forschungsvereinigung Stahlanwendung e.V. (FOSTA), Sohnstrae 65, 40237 Düsseldorf was promoted through the AiF under the program for the promotion of joint industrial (IGF) by the Federal Ministry of Economic Affairs and Energy due to a resolution of the German Bundestag. The authors want to thank the Laboratory for Materials and Joining Technology (LWF), Paderborn and Fraunhofer Institute for Manufacturing Technology and Advanced Materials (IFAM), Bremen for providing the test data.

REFERENCES

Dorfmann, A., K. Fuller, & R. Ogden (2002). Shear, compressive and dilatational response of rubberlike solids subject to cavitation damage. *INT J SOLIDS STRUCT 39*(7), 1845–1861.

Flory, P. J. (1961). Thermodynamic relations for high elastic materials. *Trans Faraday Soc 57*, 828–839.

Kachanov, L. M. (1958). Time of the rupture process under creep conditions. *Izvestia Akademii Nauk SSSR, Otdelenie Tekhnicheskich Nauk 8*, 26–31.

Lemaitre, J. (1985). A continuous damage mechanics model for ductile fracture. *J Eng Mater Techn 107*, 83–89.

Miehe, C. (1994). Aspects of the formulation and finite element implementation of large strain isotropic elasticity. *Int J Numer Meth Eng 37*, 1981–2004.